A Fluoride-Induced Aggregation Test to Quickly Assess the Efficiency of Ligand Exchange Procedures from Citrate Capped AuNPs

Maurice Retout,[‡] *Bryan Gosselin,*[‡§] *Jesse V. Jokerst,*[†] *Ivan Jabin,**[§] *and Gilles Bruylants,**[‡]

[‡] Engineering of Molecular NanoSystems, Ecole Polytechnique de Bruxelles, Université libre de Bruxelles (ULB), avenue F. D. Roosevelt 50, CP165/64, B-1050 Brussels, Belgium.

[§] Laboratoire de Chimie Organique, Université libre de Bruxelles (ULB), avenue F. D. Roosevelt 50, CP160/06, B-1050 Brussels, Belgium.

[†] Department of NanoEngineering and Department of Radiology, University of California, San Diego, La Jolla, CA 92093, United States

*Corresponding authors: Gilles.Bruylants@ulb.be; Ivan.Jabin@ulb.be

KEYWORDS: Nanomaterials - Gold nanoparticles - Functionalization - Aggregation - Fluoride

ABSTRACT

Hypothesis:

Citrate capped gold nanoparticles (AuNPs-citrate) are the starting material for most of the academic and industrial applications using gold nanoparticles. AuNPs-citrate must usually be functionalized with organic (bio)molecules, through a ligand exchange process, to become suitable for the envisaged application. The evaluation of the efficiency of the ligand-exchange process with a simple and convenient procedure is challenging.

Experiments:

Fluoride was used to evaluate the efficiency of a ligand exchange process from AuNPs-citrate with five standard types of ligands. The relationship between the aggregation level of the AuNPs exposed to fluoride and the amount of residual citrate ligands at the surface of the AuNPs was studied. The fluoride-induced aggregation process was characterized with various techniques such as TEM, UV-Vis, ATR-FTIR or MANTA and then used to quickly identify the optimal conditions for the functionalization of AuNPs-citrate with a new ligand, i.e. a PEGylated calixarene-tetradiazonium salt (X_4-$(PEG)_4$).

Findings:

It was observed that the fluoride-induced aggregation of AuNPs is proportional to the efficiency of the ligands exchange. We believe that these results could benefit to everyone engineering AuNPs for advanced applications, as the fluoride-aggregation of AuNPs can be used as a general and versatile quality test to verify the coating density of organic (bio)molecules on AuNPs.

INTRODUCTION

Due to their remarkable optical and chemical properties,[1–3] gold nanoparticles (AuNPs) have found many applications in various fields such as catalysis,[4] biosensing[5] or nanomedicine.[6–8] AuNPs are classically synthesized via the Turkevich method that gives size-controlled spherical monodisperse particles capped by citrate anions (AuNPs-citrate).[9–11] In most cases, the adsorbed citrate ligands have then to be exchanged by specific ligands that can ensure the chemical and colloidal stabilities of the AuNPs in the working conditions and bring them new properties such as biocompatibility or selective recognition.[12,13] The replacement of citrate ions by various ligands, ranging from small organic molecules[14–16] to large biomolecules,[17] has been reported in the literature.[18–20] However, the ligands exchange process is far from trivial as the citrate anions are strongly adsorbed onto the gold surface.[21] The monitoring of the ligand exchange process is thus crucial as it will dictate the performance of the AuNPs for a given application, that is strongly dependent on the ligand density at their surface.[22] The efficiency of this process depends on many experimental parameters including reaction time, temperature, concentration, pH, nature of the new ligand, etc. Besides, a lack of reproducibility may result from improper lab techniques (e.g. the use of inappropriate vial material or chemicals of insufficient quality, etc.). Furthermore, the modification of AuNPs with a ligand that has never been reported in the literature may require a painful optimization to ensure an efficient exchange of the adsorbed citrate ions. In this context, a convenient method to evaluate the ligand exchange process efficiency would be of particular interest. TGA allows to determine the organic fraction in the sample but i) it requires a lot of material, ii) it is destructive, and iii) it doesn't allow to assess the ligand exchange process if the two ligands do not greatly differ in mass. IR can provide some information,[23,24] however organic

ligands do frequently show the same absorption bands and quantitative analyses are difficult, due to the distance dependence from surface of the surface-enhanced infrared absorption effect. Advanced microscopy characterizations, as STM,[25] or mass spectrometry[26] can also be used to probe the organic coating on the surface of NPs,[27] however it is not easily accessible and cannot be considered as a routine characterization technique. A few complex methods, based on the detachment of the ligands from the surface using *aqua regia*, cyanide or iodine and their quantification using mass spectrometry or ^{1}H NMR spectroscopy, have also been reported in the literature.[22,28] To date, the characterization of the organic layer surrounding nanoparticles remains thus a scientific challenge that is unfortunately often neglected when reporting applications based on functionalized nanoparticles.

Herein, we report the development of a fast and simple method to evaluate the ligand exchange efficiency from AuNPs-citrate. It is based on the non-destructive aggregation of AuNPs induced by fluoride ions, avoiding the use of toxic cyanide ions.[23] Fluoride-induced aggregation of AuNPs has already been reported in the literature for the colorimetric detection of fluoride anions.[29–32] It involved AuNPs engineered to be sensitive to the presence of fluoride, that could cause their cross linking. However, to the best of our knowledge, it has never been used to assess the ligands exchange from citrate-capped AuNPs. We studied the use of fluoride to monitor the replacement of citrate by five types of ligands frequently used in the literature to modify AuNPs-citrate. To highlight the versatility of this technique we selected ligands differing either by the nature of their core chain, their anchoring group, or their charge. The method was then applied with success to a recently developed class of ligands, i.e. calixarene-diazonium salts. This work demonstrates how the fluoride-induced aggregation of AuNPs can be used as a simple routine quality-test to assess the functionalization of AuNPs-citrate.

RESULTS AND DISCUSSION

Effect of the addition of halides on AuNPs suspensions. Three distinct batches of 19 nm citrate-capped AuNPs (AuNPs-citrate) dispersed in aqueous solution of 1 mM citrate (OD = 8) were synthesized via a modified Turkevich method and used to replicate experiments.[9] The corresponding UV-Vis absorption spectra, TEM images and size distribution histograms can be found in the Supplementary Information (Figure S1).

First, the effect of the addition of KF on the dispersibility of the AuNPs-citrate was compared to that of the other halide salts (KCl, KBr and KI). It was observed that only the addition of fluoride led to the apparition of a second absorption peak (around 680 nm), which is the signature of particle aggregation via a Diffusion Limited Colloidal Aggregation (DLCA) mode (**Figure 1A**).[33,34] The AuNPs aggregation intensity was determined by measuring the ratio of the absorbances at 680 nm and 520 nm. This ratio was found to be proportional to the concentration of fluoride added to the AuNP suspension with a plateau appearing around 50 mM of KF (**Figure 1B**). Successive addition of KF led to an instantaneous change of color of the sample, turning progressively from red to blue at 100 mM KF (**Figure 1A**, inset). It is worth noting that the kinetics of the aggregation was fast, and that the maximum LSPR band shift was obtained in less than 20 minutes (**Figure 1C**).

The addition of chloride, bromide or iodide potassium salts also induced the aggregation of the AuNPs-citrate but the significant increase of the absorbance of the suspensions above 800 nm led to a change of color of the suspensions from red to dull grey (**Figures 1D** and **1E**). This suggests the formation of large structures possessing efficient light scattering properties. Very interestingly, the progressive addition (from 0 to 100 μM) of a thiolated PEG (HS-PEG_{16}-OCH_3,

MW= 800) to fluoride-aggregated AuNPs led to the clean redispersion of the particles and a recovery of the initial red color of the suspension (**Figure 1E**). UV-Vis spectroscopy analysis of the AuNPs dispersion after the addition of HS-PEG_{16}-OCH_3 can be found in the Supporting Information (Figure S2). Similar recovery of the colloidal dispersion from bromide, chloride or iodide-aggregated AuNPs was not observed (Figure S3). This phenomenon can be easily explained for KI as it is well known to lead to the destructive aggregation of the particles via their etching and reshaping.[35,36] TEM images of reshaped AuNPs-citrate can be seen in **Figure 1F**. However, the irreversible aggregation of AuNPs-citrate in the presence of KCl and KBr can not be explained by a destructive aggregation process as no reshaping of the AuNPs-citrate was observed by TEM (**Figure 1F**). We also verified that this effect was not due to a difference in the final pH of the suspension after addition of the halogen salt or of the thiol. According to the Derjaguin-Landau-Verwey-Overbeek (DLVO) theory,[37] the particles can be trapped in a deep energetic minima during the aggregation due to infinite Van der Waals forces, thus transforming the aggregates into larger insoluble materials that cannot be redispersed.[38,39] It is thus believed that the aggregation induced by fluoride, unlike chloride and bromide, does not lead to a permanent state of aggregation and the VdW forces remain weak enough to allow the redispersion of the particles.

Finally, neither the concentration of the AuNPs (from 0.15 nM to 3 nM) nor the concentration of citrate (from 0.2 to 20 nM) in the medium had a significant influence on the level of aggregation observed upon exposure to KF (Figures S4 and S5). Moreover, non-destructive aggregation of AuNPs in the presence of fluoride could also be observed with larger citrate-capped AuNPs: clean redispersion of fluoride-aggregated 40 nm AuNPs could also be obtained through the addition of HS-PEG_{16}-OCH_3 (100 μM) (See Figure S6).

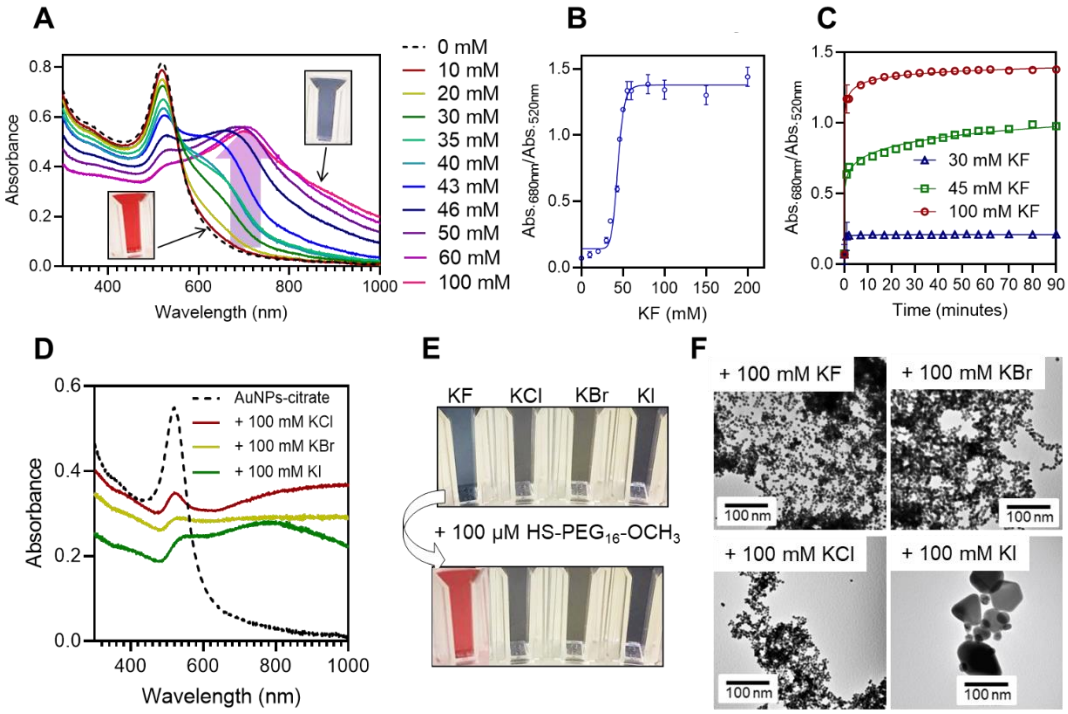

Figure 1 (A) UV-Vis spectra of AuNPs-citrate dispersed in 1 mM citrate, pH =7, 20 min after the addition of different concentrations of KF. Insets show pictures corresponding to the AuNPs-citrate before and 20 minutes after the addition of 100 mM of KF. **(B)** Ratio of the absorbances (Abs.680nm/Abs.520nm) of AuNPs-citrate as a function of KF concentration. **(C)** Evolution of the ratio Abs.680nm/Abs.520nm of AuNPs-citrate exposed to either 30 mM, 45 mM or 100 mM of KF over time. **(D)** UV-Vis spectra of AuNPs-citrate exposed to 100 mM KCl, 100 mM KBr or 100 mM KI, 20 min after the addition of different salts. **(E)** Pictures of AuNPs-citrate exposed to 100 mM of KF, KCl, KBr or KI before and after addition of 100 µM of HS-PEG_{16}-OCH_3. **(F)** TEM images of AuNPs-citrate 20 minutes after exposure to 100 mM of either KF, KBr, KCl or KI.

All these results indicate that i) the fluoride anion can interact with the citrate capped particles, either by displacing the adsorbed citrate ligands or by interacting with the adsorbed citrate molecules, triggering an aggregation of the AuNPs without degrading their metallic core, and ii) this fluoride-induced aggregation is reversible, as the addition of ligands displaying a higher affinity for AuNPs than fluoride (i.e. HS-PEG_{16}-OCH_3) leads to the redispersion of the AuNPs. The sensibility of the particles to the fluoride-induced aggregation is thus expected to be

proportional to the density of citrate molecules adsorbed at the surface of the particles. Based on this assumption, we envisioned that the fluoride-induced aggregation could be used as a non-destructive tool to evaluate the efficiency of the replacement of adsorbed citrate ions by other organic ligands.

Use of the fluoride-induced aggregation of AuNPs to evaluate the efficiency of the ligand exchange process. AuNPs carrying different densities of ligands, ranging from low coverage to full coverage of their surface, were first produced. Five ligands L1-L5, differing either by their anchoring group (a thiol, an alkyne or an aryl radical generated from an aryl diazonium),[40] the

nature of their core chain (alkane or PEG) or of their terminal functional group (OMe, OH or COOH) were investigated (**Figure 2A**).

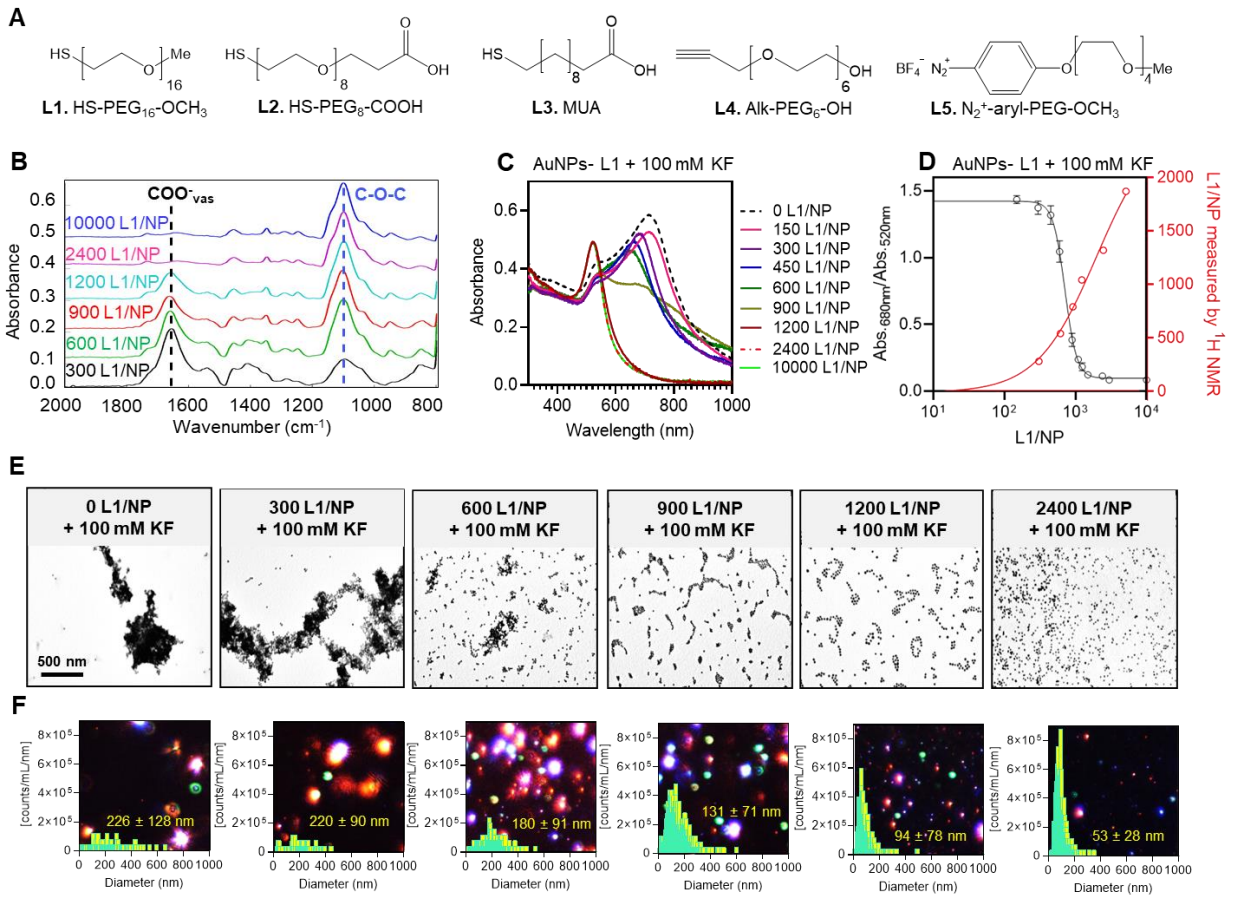

Figure 2 (A) Structures of the five ligands L1-L5 investigated. (B) ATR-FTIR spectra of AuNPs-citrate functionalized with 300, 600, 900, 1200, 2400 or 10.000 L1/NP. (C) UV-Vis spectra of AuNPs-citrate functionalized with an increasing amount of L1/NP recorded 20 minutes after the addition of 100 mM KF. (D) Ratio of the absorbances at 680 nm and 520 nm of AuNPs-citrate functionalized with 300, 600, 900, 1200 or 2400 L1/NP recorded 20 minutes after the addition of 100 mM KF and number of grafted L1 per NP determined by ^{1}H NMR spectroscopy. (E) TEM images of AuNPs-citrate functionalized with 0, 300, 600, 900, 1200 or 2400 L1/NP 20 minutes after the addition of 100 mM KF. Scale bar is 500 nm for all the images and (F) the corresponding MANTA measurements.

The proof-of-concept was demonstrated with ligand L1 as its IR bands are clearly distinct from those of citrate (i.e. C-O-C stretching from the PEG chain of L1 at 1100 cm^{-1} vs C=O

stretching from the carboxyl group of citrate at 1600 cm^{-1}). It is thus possible to observe by ATR-FTIR spectroscopy the presence of these two molecules on the AuNPs and determine their relative proportions. Different amounts of L1, in ratios ranging from hundreds to thousands of ligands per particle, were thus added to AuNPs-citrate and, after 24 hours of stirring, the resulting batches of AuNPs-L1 were cleaned from unbound citrate ions or L1 and analyzed by ATR-FTIR spectroscopy (**Figure 2B**). The intensity of the citrate signal at 1600 cm^{-1} was inversely proportional to the amount of L1 added during the exchange procedure. No more evolution of the FTIR spectrum was noticed above 2400 L1/NP and no remaining signal of citrate could be observed, indicating that the maximal density of L1 was reached. This value is in good agreement with what is reported in the literature for the functionalization density of this molecule on AuNPs-citrate via a ligand-exchange procedure.[28] It is worth noting that the spectrum of AuNPs-citrate was not plot for clarity of reading as the intensity of the citrate signals was very high, but it can be seen in the supplementary information (Figure S7).

All the batches of AuNPs-L1 were then exposed to 100 mM KF for 20 minutes and the aggregation level of the corresponding suspensions was monitored by UV-Vis spectroscopy and quantified by the ratio of the $Abs._{680nm}/Abs._{520nm}$ (**Figure 2C** and **2D**). The deformation of the LSPR band upon KF exposure was proportional to the amount of L1 added to the AuNPs-citrate. From 2400 L1/NP, the particles were not sensitive to the addition of KF (even at concentrations up to 600 mM, see Figure S8), while lower values of L1/NP led to AuNPs for which the aggregation level is linearly dependent on the presence of KF. The KF sensitivity was thus compared to the amount of L1 ligand grafted to the NPs, measured by ^{1}H NMR spectroscopy. Briefly, the supernatant of AuNPs-L1 was analyzed by ^{1}H NMR and the amount of remaining L1 ligands was quantified. This value corresponds to the non-grafted L1 and, knowing the NP

concentration, it was possible to determine the amount of grafted L1 per NP. A good correlation between the KF sensitivity (i.e. Abs. $_{680nm}$/Abs. $_{520nm}$) and the grafting density of L1 measured by ^{1}H NMR was observed (see Figure 2D). It is interesting to point out that below 1200 L1 per NP, around 90% of the ligands are grafted on the particles. Only when a sufficient density to ensure protection against KF is reached the proportion of grafted ligands start to decrease, showing a progressive saturation of the surface.

The aggregation process was then evaluated by TEM and Multispectral Advanced Nanoparticles Tracking Analysis (MANTA). TEM revealed aggregates whose size was inversely proportional to the amount of L1 used to modify the AuNPs (Figure **2E**). MANTA records video of the particles based on their light scattering of three different lasers (blue, green and red). Small particles will scatter more blue light while bigger particles will scatter more red light. Based on the images collected, MANTA counts the number of particles in the sample and determines their size. When exposed to 100 mM of KF, AuNPs-citrate aggregate and form assemblies with a size of more than 220 nm and mostly red scattering is observed on the picture. AuNPs-L1 functionalized with various amount of L1 have also been tested. The size of the aggregates was inversely proportional to the amount of L1 added on the particles (Figure **2F**). From 2400 L1/NP, no aggregation was observed and only AuNPs with a size of 53 nm were measured. This size is in good agreement with the hydrodynamic diameter of AuNPs covered with a dense HS-PEG_{16}-OCH_3 layer.

Similar experiments were conducted with the four other ligands L2-L5 (see Figures S9, S10, S11 and S12 for the UV-Vis spectra). Again, the aggregation level of the AuNPs was observed to be proportional to the number of ligands added per NP during the ligand exchange step and similar trends were observed for the plot of the absorbance ratios (Abs.$_{680nm}$/Abs.$_{520nm}$) as

a function of the fluoride concentration added in the suspension (**Figure 3**) than for ligand L1. The amount of ligands necessary to obtain the full coverage of the particle surface, indicated by the insensitivity of the particles to the presence of KF, was different from one ligand to another. The widest linear range of sensitivity to KF was observed for L3 while the shortest one was observed for L4. Values of 2200 L2/NP, 7000 L3/NP, 1700 L4/NP and 80.000 L5/NP were determined as the minimal number of equivalents of ligands per NP necessary to obtain a full coverage of the particle surface and stability of the particles against fluoride aggregation. It is worth mentioning that, in the case of L5, the high value can be explained by the different grafting chemistry that implies the reduction of the diazonium group to a highly reactive aryl radical species. Important loss of the generated activated L5 can occur through various processes, including its polymerization in solution or its reaction with the surface of the vial.

All these results show that the fluoride-induced aggregation may be used as a routine test to quickly evaluate the efficiency of a ligand exchange procedure and verify whether residual citrate ligands are still present at the surface of the nanoparticles.

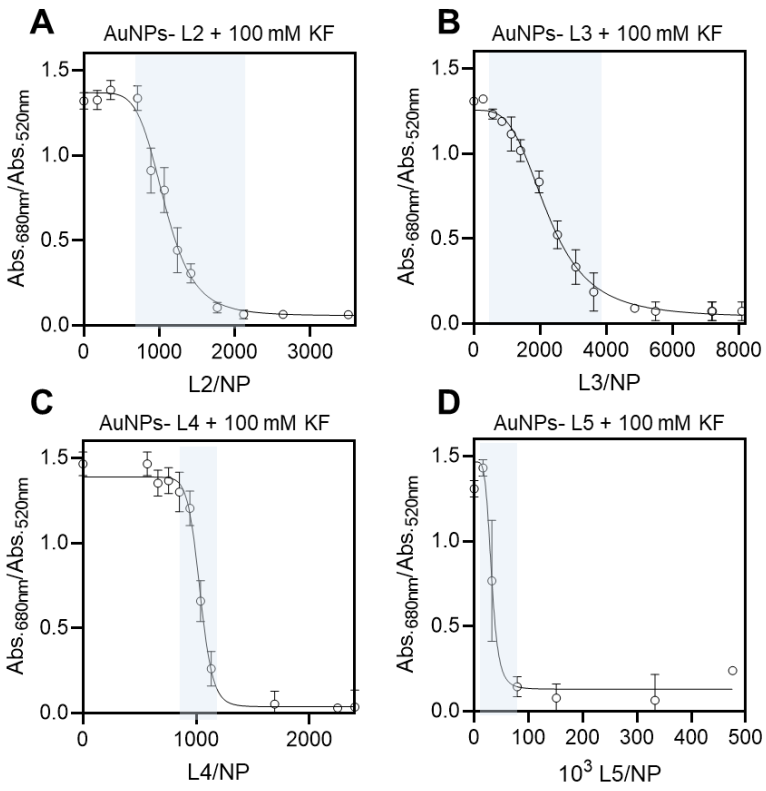

Figure 3 Ratio of the absorbance at 680 nm and 520 nm of suspensions of AuNPs functionalized with either L2 (A), L3 (B), L4 (C) or L5 (D), 20 minutes after the addition of 100 mM KF as a function of the number of ligands added per NP during the ligand exchange step. Regions highlighted in blue are those where a linear relationship is observed between the aggregation level and the amount of ligand used during the ligand exchange step.

Use of the fluoride-induced aggregation method to devise the functionalization of AuNPs with non-reported ligands. The setup of the optimal conditions for an efficient ligand exchange process usually requires the optimization of many parameters (i.e. temperature, time, concentration of the different species, pH, etc.). This is particularly true for non-reported ligands and this process might reveal time-consuming as it is difficult to distinguish NPs that present slight differences in surface ligand densities. In this context, the fluoride-induced aggregation of AuNPs could be used as a quality test to quickly discard conditions leading to inefficient ligand exchange.

To demonstrate that the fluoride-induced aggregation of AuNPs-citrate can be used to quickly optimize the functionalization conditions for non-reported ligands, we used a calix[4]arene-tetradiazonium salt bearing four PEG chains (X_4-$(PEG)_4$) at the level of its small rim (**Figure 4**), as the grafting of this compound has never been reported on AuNPs. While thiol and alkynes derivatives represent the vast majority of ligands for AuNPs functionalization, calix[4]arene-tetradiazoniums salts represent an emerging class of ligands,[41–44] that lead to an extremely stable organic coating of the particles as those macrocyclic platforms can potentially form up to four carbon-gold bonds.[14,41,45–47]

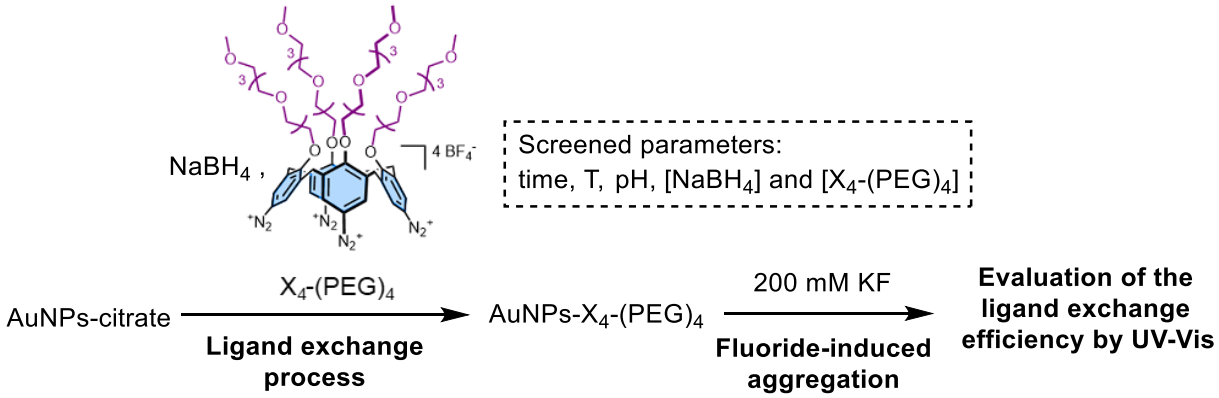

Figure 4. Use of the fluoride-induced aggregation method to optimize the functionalization of AuNPs-X_4-$(PEG)_4$.

Several functionalization parameters were screened for the optimization of the synthesis of AuNPs-X_4-$(PEG)_4$: time, temperature, pH, concentrations of X_4-$(PEG)_4$ and of the reducing agent ($NaBH_4$) (**Figure 4**). All the AuNPs batches that were produced were exposed to 200 mM KF to evaluate the ligand exchange efficiency between X_4-$(PEG)_4$ and citrate. To illustrate the usefulness of our KF test, we only present here the optimization of the quantities of reducing agent and calixarene X_4-$(PEG)_4$. The grafting of X_4-$(PEG)_4$ in the absence (spontaneous grafting) or in the presence of three different concentrations of sodium borohydride $NaBH_4$ (0.1 mM, 1 mM and 10

mM) was first evaluated. For each concentration of $NaBH_4$, different calix[4]arenes per particle ratios (i.e. 10.000, 50.000, 100.000 and 200.000) were investigated (**Table 1**).

Table 1. Different concentrations of $NaBH_4$ and X_4-$(PEG)_4$ used for the synthesis of AuNPs-X_4-$(PEG)_4$.

Conditions #	[$NaBH_4$] (mM)	[X_4-$(PEG)_4$] (amount/NP)
1	0	10.000
2	0	50.000
3	0	100.000
4	0	200.000
5	0.1	10.000
6	0.1	50.000
7	0.1	100.000
8	0.1	200.000
9	1	10.000
10	1	50.000
11	1	100.000
12	1	200.000
13	10	10.000
14	10	50.000
15	10	100.000
16	10	200.000

The absence of reducing agent as well as the use of 0.1 mM $NaBH_4$ are not suitable conditions, as the corresponding suspensions turned dark blue during the functionalization process, indicating aggregation of the particles (**Figures 5A** and **5B**). On the other hand, all the suspensions produced in the presence of 1 mM or 10 mM $NaBH_4$ did not show any variation of color over the course of the functionalization process and it was not possible to differentiate them with the naked eye (**Figures 5C** and **5D**). Moreover, UV-Vis spectroscopy cannot be used to identify the best functionalization conditions as all the spectra showed very similar LSPR bands (Figure S14). However, after the addition of 200 mM of KF, the color of five of the eight samples (i.e. conditions 9, 10, 12, 13 and 16) turned from red to purple, allowing to discard these five conditions (**Figures 5E** and **5F**).

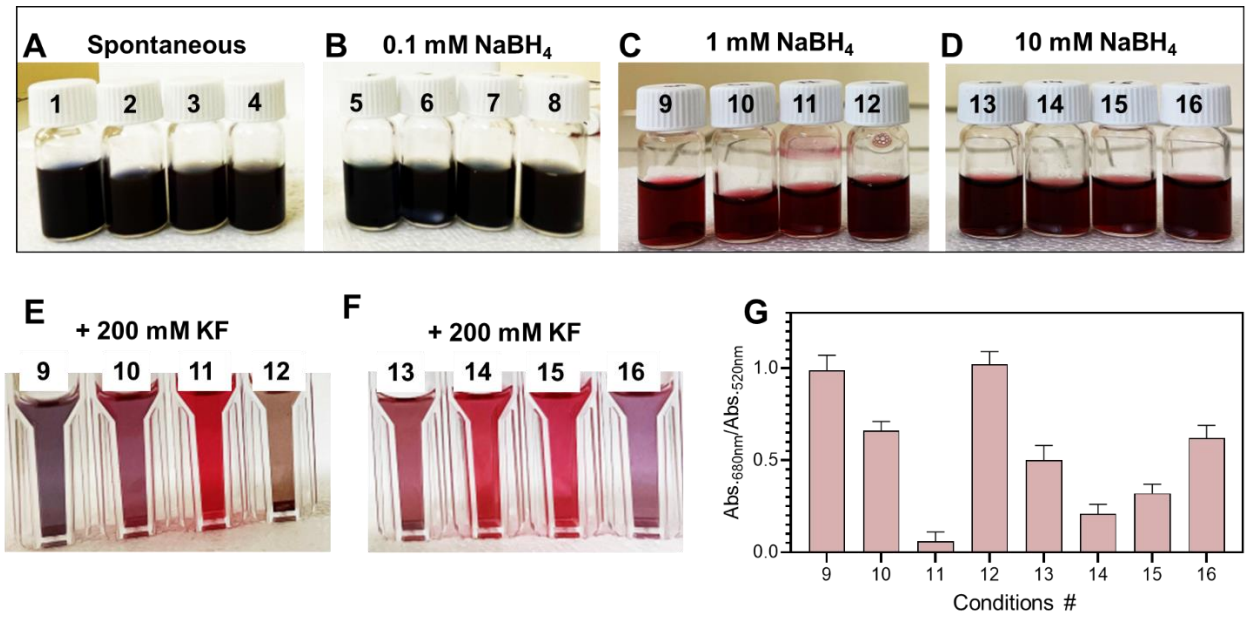

Figure 5. (A, B, C and D) Pictures of the AuNPs suspension functionalized in the 16 conditions reported in table 1. (E and F) Pictures of the AuNPs suspensions functionalized in the conditions 9, 10, 11, 12, 13, 14, 15 and 16, 20 minutes after the addition of 200 mM KF. (G) Ratio of the absorbance at 680 nm and 520 nm of AuNPs functionalized in the conditions 9, 10, 11, 12, 13, 14, 15 and 16, 20 minutes after the addition of 200 mM KF.

The three samples that remained red-colored (conditions 11, 14 and 15) could not be distinguished with the naked eye, even in the presence of fluoride. However, the aggregation intensity could be measured by UV-Vis spectroscopy and it revealed that the two samples produced in presence of 10 mM $NaBH_4$ (conditions 14 and 15) possessed a higher $Abs._{680nm}/Abs._{520nm}$ ratio than the sample produced with 1 mM $NaBH_4$ (**Figure 5G** and Figure S15). These two conditions were thus discarded. Therefore, the fluoride-induced aggregation of AuNPs allowed us to quickly determine that the optimal grafting conditions consist in 1 mM $NaBH_4$ and 100.000 equivalents of X_4-$(PEG)_4$ per particle (conditions 11). Again, this high amount of calix[4]arenes required for an optimal functionalization process is probably inherent to the grafting process with aryl diazonium species (*vide supra*). AuNPs-X_4-$(PEG)_4$ made under these

optimal conditions possess excellent chemical and colloidal stabilities (Figure S16). They could be easily cleaned from excess reagents and further characterization by IR and UV-Vis spectroscopy confirmed the presence of the calixarene ligand at their surface and the removal of citrate anions (Figures S17 and S18).

CONCLUSION

In this work, we aimed to develop a routine methodology to assess the ligand exchange efficiency while replacing citrate ions from AuNPs surface with other ligands, as most of the actual characterization methods are complex or time-consuming. In a first step, we studied the effect of the addition of halides on AuNPs-citrate. We observed that fluoride anions distinguish themselves from the other halides (Cl^-, Br^- and I^-) by the absence of degradation of the nanoparticle metallic core; only a reversible aggregation of the AuNPs via a DLCA mode was observed upon the addition of KF and the addition of thiolated PEG ligand could redisperse the fluoride-aggregated AuNPs regardless of their size (20 nm or 40 nm). This non-destructive fluoride-induced aggregation of AuNPs-citrate was then exploited to evaluate the ligand exchange efficiency of five standard types of ligands differing either by their core, size, or anchoring group. In all cases, it was observed that the fluoride-induced aggregation intensity was proportional to the level of residual citrate ligands at the surface of the AuNPs. Finally, the fluoride-aggregation method was used successfully to optimize the functionalization of AuNPs-citrate with a ligand never reported in the literature, i.e. a PEGylated calixarene-tetradiazonium salt (X_4-$(PEG)_4$). Conditions leading to the optimal coating of AuNPs with X_4-$(PEG)_4$ were easily and quickly found by trial-error experiments, the fluoride-aggregation method enabling to quickly discard conditions leading to poorly coated particles. We think that these results could benefit to everyone investigating the

functionalization of AuNPs as the fluoride-aggregation of AuNPs can be used as a quality test to simply verify the coating of AuNPs.

EXPERIMENTAL SECTION

General materials. Potassium gold (III) tetrachloride ($KAuCl_4$), tetrachloroauric acid ($HAuCl_4$), trisodium citrate ($Na_3C_6H_5O_7$), mercaptoundecanoic acid (MUA) (purity of 98%) and Poly(ethylene glycol) methyl ether thiol ($HS\text{-}PEG_{16}\text{-}OCH_3$, Mw = 800 Da) (purity of 95%) were purchased from Sigma-Aldrich (St-Louis, MO) and alpha-thio-omega-(propionic acid) octa(ethylene glycol) ($HS\text{-}PEG_8\text{-}COOH$, Mw = 458 Da) was ordered from Iris Biotech GMBH with a purity of 95%. Alkyne PEG hydroxy ($Alk\text{-}PEG_6\text{-}OH$, Mw = 380 Da) was purchased from PurePEG, LLC (San Diego, CA). Potassium iodide, potassium bromide, potassium chloride and potassium fluoride were purchased from VWR (Radnor, Penn). Calix[4]arene $X_4\text{-}(PEG)_4$ was synthesized according to procedures reported in the literature.[48] Before use, all glassware and Teflon-coated stir bars were washed with aqua regia (3:1 volume ratio of concentrated HCl and HNO_3) and rinsed thoroughly with water.

Caution! Although we have not encountered any problem, it is noted that diazonium salt derivatives are potentially explosive and should be handled with appropriate precautions. Aqua regia is highly toxic and corrosive and requires proper personal protective equipment. Aqua regia should only be handled in a fume hood.

Gold nanoparticles synthesis. Three batches of citrate-capped gold nanoparticles (AuNPs-citrate) were synthesized in an aqueous solution using a modified Turkevich method.[42] Briefly, in a three-neck round-bottom flask, 1.4 mL of a 0.15 M trisodium citrate solution were injected into 50 mL of boiling aqueous potassium gold (III) tetrachloride (3 mM) at pH7. After addition, the reaction

mixture changed from yellow to colorless, then to black and finally to purple-red within 1 minute. The solution was kept under reflux for five minutes and then quenched to room temperature using cold water. The freshly synthesized AuNPs-citrate suspension was then dialyzed twice against 1 mM citrate solutions for 12 hours.

Use of the fluoride-induced aggregation of AuNPs to evaluate the efficiency of the ligand exchange process. Fresh ligand solutions (0.5 mM) were prepared by dissolving the ligand in the appropriate solvent: water for HS-PEG_{16}-OCH_3, HS-PEG_8-COOH, Alk-PEG_6-OH and methanol for MUA. The general procedure was the following for each ligand: several batches of 2 mL of AuNPs suspension (5 nM) were prepared in a glass vial with magnetic stirrer. To this, an appropriate volume of the ligand solution (0.5 mM) was added to reach the desired density (ligands/NP) and the reaction mixture was stirred for approximately 16 hours at room temperature. At the end of the reaction, 200 µL of the modified AuNPs were dispersed in 1 mL of water in a disposable cuvette and a UV-Vis spectrum was recorded. 25 µL of KF (aqueous 4M) was then added. 20 minutes later, another UV-Vis spectrum was recorded and the ratio between the absorbances at 680 nm and 520 nm was measured.

Optimal condition of calixarene grafting on AuNPs. First, calixarene-diazonium salts was dissolved in pure water to make a 5 mM aqueous solution and the pH was increased to 4.5 through the addition of appropriate volume of an aqueous NaOH solution (1M). In a glass vial with a magnetic stirrer, 20 µL of $NaBH_4$ (0.1M) was added to 2 mL of AuNPs suspension (5 nM). Directly after this, 200 µL of the calixarene solution were added slowly (approximately 20 seconds for the complete addition). Formation of foam was sometimes observed. After 16 hours of reaction, 200 µL of AuNPs-calixarene were used for the functionalization density testing with fluoride (see above) and the rest was cleaned from excess of reagents by centrifugation at 18.000g for 20

minutes. Four cycles of centrifugation were required to ensure the complete removing of reagents. For the two first cycles, the supernatant was replaced by a sodium dodecylsulfate solution (1% in mass) while for the two last, it was replaced by water.

UV-Vis spectroscopy. UV-Vis absorption spectra were recorded from 1000 to 300 nm at a 120 nm/min scan speed with a UV Vis-NIR spectrophotometer in disposable (PMMA) cuvettes with a 1 cm optical path length at room temperature.

Attenuated Total Reflection Fourier-transform Infrared. Attenuated Total Reflection Fourier-transform Infrared **(**ATR-FTIR) spectra were recorded at 22 °C on a FTIR spectrophotometer equipped with a liquid-nitrogen-cooled mercury−cadmium−telluride detector. The spectrophotometer was continuously purged with dried air. The solutions/suspensions were deposited on a germanium single-crystal internal reflection element (triangular prism of 6.8 × 45 mm, with an internal incidence angle of 45°), and the solvent was removed with a flow of dry nitrogen gas. Bare germanium was used for the background spectrum. Opus software (4.2.37) was used to record 128 scans with a nominal resolution of 2 cm^{-1}. Data were processed and analyzed using the home written Kinetics package in Matlab R2013a by subtraction of water vapor, baseline correction, and apodization at 10 cm^{-1}.

Transmission Electron Microscopy. Images of the AuNPs were obtained with a Philips CM20-UltraTWIN Transmission Electron Microscope (TEM) equipped with a lanthanum hexaboride (LaB6) crystal at a 200kV accelerating voltage. The average size and 95% confidence interval were determined by measuring the size of more than 100 AuNPs.

Multispectral Advanced Nanoparticles Tracking Analysis (MANTA). The multispectral advanced nanoparticle tracking analysis (MANTA) is a technique that builds images from the particles light scattering via three lasers of different wavelengths (e.g., blue, green, and red); the

wavelength of scattering depends on nanoparticle size. Thus, small particles (<100 nm) appear blue while larger particles appear green or red. MANTA uses these images to count the nanoparticles and calculate their size based on Brownian motion. MANTA was performed with the ViewSizer 3000 (Horiba Scientific, USA). The temperature was set to 25 °C during the measurement. Automated noise analysis determines the optimal wavelength for representing each nanoparticle. Here, 8-bit composite videos were generated, and 10 videos were used per analysis (300 frames for seconds). A quartz cuvette with minimum volume of 1 mL was used for the measurement and the AuNPs concentrations was set up at 0.04 nM.

^{1}H NMR spectroscopy. Quantification of the L1 grafting densities on the AuNPs by 1H NMR was performed on a Varian Unity 600 MHz spectrometer, by determining the amounts of non-grafted L1 in the supernatant after centrifugation of the particles. 1D proton spectra were recorded at 25 °C with 128 transients, an acquisition time of 2 s, a relaxation delay of 13 s, a spectral width of 9600 Hz, and a digital resolution of at least 0.2 Hz/pt. The chemical shift of water at 25 °C (4.79 ppm) was used as chemical shift reference. Signal at 3.8 ppm coming from the 64 protons of the PEG chain of L1 was used for the quantification and compared to the signal of the 6 protons of DMSO. It is worth to mention that the supernatant was dried and the water was replaced by D_2O.

ASSOCIATED CONTENT

Supporting information. UV-Vis spectra of three batches of 19 nm AuNPs-citrate with corresponding TEM images and size-distribution histograms. UV-vis spectrum of fluoride-aggregated 40 nm AuNPs-citrate. UV-Vis spectra of different batches of AuNPs modified with different amount of ligands after addition of KF. UV-Vis spectra of AuNPs modified with different

amount of calixarenes in different reducing conditions before and after the addition of KF. ATR-FTIR spectra of AuNPs-X_4-$(PEG)_4$. UV-Vis spectrum of AuNPs-X_4-$(PEG)_4$.

ACKNOWLEDGMENTS

This research was supported by the Fonds pour la formation à la Recherche dans l'Industrie et dans l'Agriculture (FRIA-FRS) (PhD grant to B.G.), the "Actions de Recherches Concertées" of the Fédération Wallonie-Bruxelles and the ULB (Ph.D. grant to M. R.). J.V.J. thanks the National Institutes of Health (S10 OD023555) for the MANTA analysis work.

AUTHOR INFORMATION

Corresponding Authors

*E-mail: Gilles.Bruylants@ulb.be; Ivan.Jabin@ulb.be

Conflicts of interest

All authors declare that they have no conflict of interest.

RFERENCES

(1) Sharifi, M.; Attar, F.; Saboury, A. A.; Akhtari, K.; Hooshmand, N.; Hasan, A.; El-Sayed, M. A.; Falahati, M. Plasmonic Gold Nanoparticles: Optical Manipulation, Imaging, Drug Delivery and Therapy. *Journal of Controlled Release* **2019**, *311–312* (June), 170–189. https://doi.org/10.1016/j.jconrel.2019.08.032.

(2) Kailasa, S. K.; Koduru, J. R.; Desai, M. L.; Park, T. J.; Singhal, R. K.; Basu, H. Recent Progress on Surface Chemistry of Plasmonic Metal Nanoparticles for Colorimetric Assay of Drugs in Pharmaceutical and Biological Samples. *TrAC - Trends in Analytical Chemistry* **2018**, *105*, 106–120. https://doi.org/10.1016/j.trac.2018.05.004.

(3) Kelly, K. L.; Coronado, E.; Zhao, L. L.; Schatz, G. C. The Optical Properties of Metal Nanoparticles: The Influence of Size, Shape, and Dielectric Environment. *Journal of Physical Chemistry B* **2003**, *107* (3), 668–677. https://doi.org/10.1021/jp026731y.

(4) Que, Y.; Feng, C.; Zhang, S.; Huang, X. Stability and Catalytic Activity of PEG- b -PS-Capped Gold Nanoparticles: A Matter of PS Chain Length. *The Journal of Physical Chemistry C* **2015**, *119*, 1960–1970. https://doi.org/10.1021/jp511850v.

(5) Chang, C. C.; Chen, C. P.; Wu, T. H.; Yang, C. H.; Lin, C. W.; Chen, C. Y. Gold Nanoparticle-Based Colorimetric Strategies for Chemical and Biological Sensing Applications. *Nanomaterials* **2019**, *9* (6), 1–24. https://doi.org/10.3390/nano9060861.

(6) Khlebtsov, N. G.; Dykman, L. A. Optical Properties and Biomedical Applications of Plasmonic Nanoparticles. *J Quant Spectrosc Radiat Transf* **2010**, *111* (1), 1–35. https://doi.org/10.1016/j.jqsrt.2009.07.012.

(7) Bansal, S. A.; Kumar, V.; Karimi, J.; Singh, A. P.; Kumar, S. Role of Gold Nanoparticles in Advanced Biomedical Applications. *Nanoscale Adv* **2020**, *2* (9), 3764–3787. https://doi.org/10.1039/d0na00472c.

(8) Cordeiro, M.; Carlos, F. F.; Pedrosa, P.; Lopez, A.; Baptista, P. V. Gold Nanoparticles for Diagnostics: Advances towards Points of Care. *Diagnostics* **2016**, *6* (4). https://doi.org/10.3390/diagnostics6040043.

(9) Doyen, M.; Bartik, K.; Bruylants, G. UV-Vis and NMR Study of the Formation of Gold Nanoparticles by Citrate Reduction: Observation of Gold-Citrate Aggregates. *J Colloid Interface Sci* **2013**, *399*, 1–5. https://doi.org/10.1016/j.jcis.2013.02.040.

(10) Zhao, P.; Li, N.; Astruc, D. State of the Art in Gold Nanoparticle Synthesis. *Coord Chem Rev* **2013**, *257* (3–4), 638–665. https://doi.org/10.1016/j.ccr.2012.09.002.

(11) Kimling, J.; Maier, M.; Okenve, B.; Kotaidis, V.; Ballot, H.; Plech, A. Turkevich Method for Gold Nanoparticle Synthesis Revisited. *Journal of Physical Chemistry B* **2006**, *110* (32), 15700–15707. https://doi.org/10.1021/jp061667w.

(12) António, M.; Nogueira, J.; Vitorino, R.; Daniel-da-silva, A. L. Functionalized Gold Nanoparticles for the Detection of C-Reactive Protein. *Nanomaterials* **2018**, *8* (4), 1–21. https://doi.org/10.3390/nano8040200.

(13) Zhou, J.; Ralston, J.; Sedev, R.; Beattie, D. A. Functionalized Gold Nanoparticles: Synthesis, Structure and Colloid Stability. *J Colloid Interface Sci* **2009**, *331* (2), 251–262. https://doi.org/10.1016/j.jcis.2008.12.002.

(14) Retout, M.; Blond, P.; Jabin, I.; Bruylants, G. Ultrastable PEGylated Calixarene-Coated Gold Nanoparticles with a Tunable Bioconjugation Density for Biosensing Applications. *Bioconjug Chem* **2021**, *32*, 290–300. https://doi.org/10.1021/acs.bioconjchem.0c00669.

(15) Jin, Z.; Mantri, Y.; Retout, M.; Cheng, Y.; Zhou, J.; Jorns, A.; Fajtova, P.; Yim, W.; Moore, C.; Xu, M.; Creyer, M.; Borum, R.; Zhou, J.; Wu, Z.; He, T.; Penny, W.; O'Donoghue, A.; Jokerst, J. A Charge-Switchable Zwitterionic Peptide for Rapid Detection of SARS-CoV-2

Main Protease. *Angewandte Chemie International Edition* **2022**, *61*. https://doi.org/10.1002/anie.202112995.

(16) Ishida, Y.; Suzuki, J.; Akita, I.; Yonezawa, T. Ultrarapid Cationization of Gold Nanoparticles via a Single-Step Ligand Exchange Reaction. *Langmuir* **2018**, *34* (36), 10668–10672. https://doi.org/10.1021/acs.langmuir.8b02226.

(17) Retout, M.; Valkenier, H.; Triffaux, E.; Doneux, T.; Bartik, K.; Bruylants, G. Rapid and Selective Detection of Proteins by Dual Trapping Using Gold Nanoparticles Functionalized with Peptide Aptamers. *ACS Sens* **2016**, *1*, 929–933. https://doi.org/10.1021/acssensors.6b00229.

(18) Häkkinen, H. The Gold-Sulfur Interface at the Nanoscale. *Nat Chem* **2012**, *4*, 443–455. https://doi.org/10.1038/nchem.1352.

(19) Sandström, P.; Boncheva, M.; Åkerman, B. Nonspecific and Thiol-Specific Binding of DNA to Gold Nanoparticles. *Langmuir* **2003**, *19* (18), 7537–7543. https://doi.org/10.1021/la034348u.

(20) Woehrle, G. H.; Brown, L. O.; Hutchison, J. E. Thiol-Functionalized, 1.5-Nm Gold Nanoparticles through Ligand Exchange Reactions: Scope and Mechanism of Ligand Exchange. *J Am Chem Soc* **2005**, *127* (7), 2172–2183. https://doi.org/10.1021/ja0457718.

(21) Koyama, N.; Akiyama, T.; Oku, T. Fabrication and Surface-Enhanced Raman Scattering Properties of Thin-Film Assemblies of Classified Silver Nanoparticles. *Jpn J Appl Phys* **2021**, *60* (2). https://doi.org/10.35848/1347-4065/abd36c.

(22) Smith, M. C.; Crist, R. M.; Clogston, J. D.; Mcneil, S. E. Quantitative Analysis of PEG-Functionalized Colloidal Gold Nanoparticles Using Charged Aerosol Detection. *Anal Bioanal Chem* **2015**, *407*, 3705–3716. https://doi.org/10.1007/s00216-015-8589-2.

(23) Schulz, F.; Dahl, G. T.; Besztejan, S.; Schroer, M. A.; Lehmkühler, F.; Grübel, G.; Vossmeyer, T.; Lange, H. Ligand Layer Engineering to Control Stability and Interfacial Properties of Nanoparticles. *Langmuir* **2016**, *32* (31), 7897–7907. https://doi.org/10.1021/acs.langmuir.6b01704.

(24) Valkenier, H.; Malytskyi, V.; Blond, P.; Retout, M.; Mattiuzzi, A.; Goole, J.; Raussens, V.; Jabin, I.; Bruylants, G. Controlled Functionalization of Gold Nanoparticles with Mixtures of Calix[4]Arenes Revealed by Infrared Spectroscopy. *Langmuir* **2017**, *33*, 8253–8259. https://doi.org/10.1021/acs.langmuir.7b02140.

(25) Jackson, A. M.; Myerson, J. W.; Stellacci, F. Spontaneous Assembly of Subnanometre-Ordered Domains in the Ligand Shell of Monolayer-Protected Nanoparticles. *Nat Mater* **2004**, *3* (5), 330–336. https://doi.org/10.1038/nmat1116.

(26) Harkness, K. M.; Balinski, A.; McLean, J. A.; Cliffel, D. E. Nanoscale Phase Segregation of Mixed Thiolates on Gold Nanoparticles. *Angewandte Chemie - International Edition* **2011**, *50* (45), 10554–10559. https://doi.org/10.1002/anie.201102882.

(27) Ong, Q.; Luo, Z.; Stellacci, F. Characterization of Ligand Shell for Mixed-Ligand Coated Gold Nanoparticles. *Acc Chem Res* **2017**, *50* (8), 1911–1919. https://doi.org/10.1021/acs.accounts.7b00165.

(28) Retout, M.; Brunetti, E.; Valkenier, H.; Bruylants, G. Limits of Thiol Chemistry Revealed by Quantitative Analysis of Mixed Layers of Thiolated-PEG Ligands Grafted onto Gold Nanoparticles. *J Colloid Interface Sci* **2019**, *557*, 807–815. https://doi.org/10.1016/j.jcis.2019.09.047.

(29) Gu, J.; Lin, Y.; Chia, Y.; Lin, H. Colorimetric and Bare-Eye Determination of Fluoride Using Gold Nanoparticle Agglomeration Probes. *Microchimica Acta*, **2013**, *80*, 801–806. https://doi.org/10.1007/s00604-013-0972-0.

(30) Watanabe, S.; Seguchi, H.; Yoshida, K.; Kifune, K.; Tadaki, T.; Shiozaki, H. Colorimetric Detection of Fluoride Ion in an Aqueous Solution Using a Thioglucose-Capped Gold Nanoparticle. *Tetrahedron Lett* **2005**, *46* (51), 8827–8829. https://doi.org/10.1016/j.tetlet.2005.10.097.

(31) Jayeoye, T. J.; Rujiralai, T. Sensitive and Selective Colorimetric Probe for Fluoride Detection Based on the Interaction between 3-Aminophenylboronic Acid and Dithiobis(Succinimidylpropionate) Modified Gold Nanoparticles. *New Journal of Chemistry* **2020**, *44* (15), 5711–5719. https://doi.org/10.1039/d0nj00897d.

(32) Sun, J. F.; Liu, R.; Zhang, Z. M.; Liu, J. F. Incorporation of the Fluoride Induced SiO Bond Cleavage and Functionalized Gold Nanoparticle Aggregation into One Colorimetric Probe for Highly Specific and Sensitive Detection of Fluoride. *Anal Chim Acta* **2014**, *820*, 139–145. https://doi.org/10.1016/j.aca.2014.02.026.

(33) Doyen, M.; Goole, J.; Bartik, K.; Bruylants, G. Amino Acid Induced Fractal Aggregation of Gold Nanoparticles: Why and How. *J Colloid Interface Sci* **2016**, *464*, 60–166. https://doi.org/10.1016/j.jcis.2015.11.017.

(34) Lin, M. Y.; Lindsay, H. M.; Weitz, D. A.; Ball, R. C.; Klein, R.; Meakin, P. Universality in Colloid Aggregation. *Nature* **1989**, *339*, 360–362.

(35) Wang, J.; Li, Y. F.; Huang, C. Z. Identification of Iodine-Induced Morphological Transformation of Gold Nanorods. *Journal of Physical Chemistry C* **2008**, *112*, 11691–11695. https://doi.org/10.1021/jp801993n.

(36) Sun, S.; Gao, M.; Lei, G.; Zou, H.; Ma, J.; Huang, C. Visually Monitoring the Etching Process of Gold Nanoparticles by KI/I2 at Single-Nanoparticle Level Using Scattered-Light Dark-Field Microscopic Imaging. *Nano Res* **2016**, *9*, 1125–1134. https://doi.org/10.1007/s12274-016-1007-z.

(37) Derjaguin, V.; Churaev N.V.; Muller V. M. The Derjaguin-Landau-Verwey-Overbeek (DLVO) Theory Stability of Lyophobic Colloids **1987** *In: Surface Forces*. Springer, Boston, MA. https://doi.org/10.1007/978-1-4757-6639-4_8

(38) Mani, E.; Lechner, W.; Kegel, W. K.; Bolhuis, P. G. Equilibrium and Non-Equilibrium Cluster Phases in Colloids with Competing Interactions. *Soft Matter* **2014**, *10* (25), 4479–4486. https://doi.org/10.1039/c3sm53058b.

(39) Retout, M.; Jin, Z.; Tsujimoto, J.; Mantri, Y.; Borum, R.; Creyer, M.; Yim, W.; He, T.; Chang, Y.-C.; Jokerst, J. Di-Arginine Additives for Dissociation of Gold Nanoparticle Aggregates: A Matrix-Insensitive Approach with Applications in Protease Detection. *ACS Appl Mater Interfaces* **2022**, *14*, 52553–52565.

(40) Pinson, J.; Podvorica, F. Attachment of Organic Layers to Conductive or Semiconductive Surfaces by Reduction of Diazonium Salts. *Chem. Soc. Rev.* **2005**, *34*, 429–439. https://doi.org/10.1039/B406228K

(41) Ludovic Troian-Gautier; Valkenier, H.; Mattiuzzi, A.; Jabin, I.; van den Brande, N.; van Mele, B.; Hubert, J.; Reniers, F.; Bruylants, G.; Lagrost, C.; Leroux, Y. Extremely Robust and Post-Functionalizable Gold Nanoparticles Coated with Calix[4]Arenes via Metal–Carbon Bonds. *Chem. Commun.* **2016**, *52*, 10493–10496. https://doi.org/10.1039/c6cc04534k.

(42) Retout, M.; Gosselin, B.; Mattiuzzi, A.; Ternad, I.; Jabin, I.; Bruylants, G. Peptide-Conjugated Silver Nanoparticles for the Colorimetric Detection of the Oncoprotein Mdm2 in Human Serum. *Chempluschem* **2022**, 1–8. https://doi.org/10.1002/cplu.202200043.

(43) Gosselin, B.; Retout, M.; Troian-gautier, L.; Bevernaegie, R.; Denis, O.; Bruylants, G.; Jabin, I.; Herens, S.; Lefe, P. Ultrastable Silver Nanoparticles for Rapid Serology Detection of Anti-SARS-CoV-2 Immunoglobulins G. *Anal Chem* **2022**, *94*, 7383–7390. https://doi.org/10.1021/acs.analchem.2c00870.

(44) Retout, M.; Cornelio, B.; Bruylants, G.; Jabin, I. Bifunctional Calix[4]Arene-Coated Gold Nanoparticles for Orthogonal Conjugation. *Langmuir* **2022**, *38*, 9301–9309. https://doi.org/10.1021/acs.langmuir.2c01122

(45) Blond, P.; Bevernaegie, R.; Troian-Gautier, L.; Lagrost, C.; Hubert, J.; Reniers, F.; Raussens, V.; Jabin, I. Ready-to-Use Germanium Surfaces for the Development of FTIR-Based Biosensors for Proteins. *Langmuir* **2020**, *36*, 12068–12076. https://doi.org/10.1021/acs.langmuir.0c02681.

(46) Santos, L.; Mattiuzzi, A.; Jabin, I.; Vandencasteele, N.; Reniers, F.; Reinaud, O.; Hapiot, P.; Lhenry, S.; Leroux, Y.; Lagrost, C. One-Pot Electrografting of Mixed Monolayers with Controlled Composition. *J. Phys. Chem. C* **2014**, *118* (29), 15919–15928. https://doi.org/10.1021/jp5052003.

(47) Retout, M.; Jabin, I.; Bruylants, G. Synthesis of Ultrastable and Bioconjugable Ag, Au, and Bimetallic Ag_Au Nanoparticles Coated with Calix[4]Arenes. *ACS Omega* **2021**, *6*, 19675–19684. https://doi.org/https://doi.org/10.1021/acsomega.1c02327.

(48) Blond, P.; Mattiuzzi, A.; Valkenier, H.; Troian-Gautier, L.; Bergamini, J. F.; Doneux, T.; Goormaghtigh, E.; Raussens, V.; Jabin, I. Grafting of Oligo(Ethylene Glycol)-Functionalized Calix[4]Arene-Tetradiazonium Salts for Antifouling Germanium and Gold

Surfaces. *Langmuir* **2018**, *34* (21), 6021–6027. https://doi.org/10.1021/acs.langmuir.8b00464.